HHS Public Access

Author manuscript

Proc SPIE Int Soc Opt Eng. Author manuscript; available in PMC 2024 March 18.

Published in final edited form as:

Proc SPIE Int Soc Opt Eng. 2024 February ; 12463: . doi:10.1117/12.2654431.

Super-resolution reconstruction of γ-ray CT images for PET-enabled dual-energy CT imaging

Yansong Zhu[a], **Benjamin A. Spencer**[a,b], **Zhaoheng Xie**[b], **Edwin K. Leung**[c], **Reimund Bayerlein**[a], **Negar Omidvari**[b], **Simon R. Cherry**[b,a], **Jinyi Qi**[b], **Ramsey D. Badawi**[a,b], **Guobao Wang**[a]

[a]Department of Radiology, University of California Davis Medical Center, Sacramento, CA, 95817, USA

[b]Department of Biomedical Engineering, University of California Davis, Davis, CA, 95616, USA

[c]UIH America, Inc., Houston, TX, 77054, USA

Abstract

Dual-energy computed tomography (DECT) enables material decomposition for tissues and produces additional information for PET/CT imaging to potentially improve the characterization of diseases. PET-enabled DECT (PDECT) allows the generation of PET and DECT images simultaneously with a conventional PET/CT scanner without the need for a second x-ray CT scan. In PDECT, high-energy γ-ray CT (GCT) images at 511 keV are obtained from time-of-flight (TOF) PET data and are combined with the existing x-ray CT images to form DECT imaging. We have developed a kernel-based maximum-likelihood attenuation and activity (MLAA) method that uses x-ray CT images as a priori information for noise suppression. However, our previous studies focused on GCT image reconstruction at the PET image resolution which is coarser than the image resolution of the x-ray CT. In this work, we explored the feasibility of generating super-resolution GCT images at the corresponding CT resolution. The study was conducted using both phantom and patient scans acquired with the uEXPLORER total-body PET/CT system. GCT images at the PET resolution with a pixel size of 4.0 mm × 4.0 mm and at the CT resolution with a pixel size of 1.2 mm × 1.2 mm were reconstructed using both the standard MLAA and kernel MLAA methods. The results indicated that the GCT images at the CT resolution had sharper edges and revealed more structural details compared to the images reconstructed at the PET resolution. Furthermore, images from the kernel MLAA method showed substantially improved image quality compared to those obtained with the standard MLAA method.

Keywords

PET-enabled dual-energy CT; super-resolution; kernel MLAA; phantom study; patient study

Further author information: (Send correspondence to Yansong Zhu) yszhu@ucdavis.edu.

1. INTRODUCTION

Dual-energy computed tomography (DECT) enables material decomposition for tissues and produces additional information for PET/CT imaging to potentially improve the characterization of diseases. However, combining DECT with a conventional PET/CT system can be challenging. DECT increases radiation dose due to the need for a second x-ray CT scan, and may not be available on most conventional PET/CT systems.

PET-enabled DECT (PDECT) has recently been proposed[1,2]. It enables simultaneous generation of PET and DECT images with a conventional PET/CT scanner without the need for a second x-ray CT scan. In PDECT, high-energy γ-ray CT (GCT) images at 511 keV are obtained from time-of-flight (TOF) PET data and are combined with the existing x-ray CT images to form DECT images.

To obtain high quality GCT images, we have previously developed a kernel-based maximum-likelihood attenuation and activity (MLAA) method that used x-ray CT images as a priori information to guide the reconstruction of GCT images. The method had shown substantially improved image quality, particularly with respect to noise suppression, compared to the standard MLAA method[3]. In previous work, however, the reconstructed GCT images were limited to the PET image resolution, for example, a 4 mm reconstructed isotropic pixel size[1], which is coarser than the x-ray CT image resolution (e.g., 1 mm reconstructed isotropic voxel size). The GCT images reconstructed based on the PET resolution may compromise the performance of PDECT.

In this work, we explored the feasibility of generating super-resolution GCT images from PET data at a much finer resolution than the PET resolution, achieved by exploiting the high-resolution prior information obtained from the x-ray CT. We evaluated the super-resolution GCT image reconstructions using phantom and patient data acquired from a uEXPLORER total-body PET/CT system.

2. METHODS

2.1 Kernel MLAA with the PET resolution

To obtain GCT images from the TOF PET emission data, methods for joint estimation of activity and attenuation can be applied. The standard MLAA algorithm seeks to solve[3]:

$$\widehat{\boldsymbol{\lambda}}, \widehat{\boldsymbol{\mu}} = \underset{\boldsymbol{\lambda} \geq \mathbf{0}, \boldsymbol{\mu} \geq \mathbf{0}}{\operatorname{argmax}} \; L(\boldsymbol{y} \mid \boldsymbol{\lambda}, \boldsymbol{\mu}), \tag{1}$$

where $\boldsymbol{\lambda}$, $\boldsymbol{\mu}$ are the PET activity and 511 keV GCT attenuation images at the low PET resolution (LR) to be estimated, respectively; $\boldsymbol{y}$ denotes PET emission measurements; and L is the Poisson log-likelihood function for the TOF PET data.

The kernel MLAA method utilizes a kernel representation which describes the GCT image as:

$$\boldsymbol{\mu} = \boldsymbol{K}(\boldsymbol{\mu}_{CT}^{LR})\boldsymbol{\alpha}, \tag{2}$$

where $\boldsymbol{K}$ is a kernel matrix built from the x-ray CT image prior $\boldsymbol{\mu}_{CT}^{LR}$ at the PET resolution. The kernel coefficient image $\boldsymbol{\alpha}$ is then jointly estimated with the PET activity image $\boldsymbol{\lambda}$ using:

$$\widehat{\boldsymbol{\lambda}}, \widehat{\boldsymbol{\alpha}} = \underset{\boldsymbol{\lambda} \geq \mathbf{0}, \boldsymbol{\alpha} \geq \mathbf{0}}{\operatorname{argmax}} \; L(\boldsymbol{y} \mid \boldsymbol{\lambda}, \boldsymbol{K}(\boldsymbol{\mu}_{CT}^{LR})\boldsymbol{\alpha}). \tag{3}$$

The final GCT image is obtained as $\widehat{\boldsymbol{\mu}} = \boldsymbol{K}(\boldsymbol{\mu}_{CT}^{LR})\widehat{\boldsymbol{\alpha}}$. When $\boldsymbol{K}$ is set to the identity matrix, the kernel MLAA is equivalent to the standard MLAA in [3].

2.2 Proposed super-resolution kernel MLAA

To generate super-resolution GCT images $\boldsymbol{\mu}^{SR}$, kernel matrix $\boldsymbol{K}$ is built directly from the x-ray CT images at the high CT resolution, with its (m, n)th element as:

$$\kappa(\boldsymbol{f}_m, \boldsymbol{f}_n) = \exp\left(-\frac{\|\boldsymbol{f}_m - \boldsymbol{f}_n\|^2}{2\sigma}\right), \tag{4}$$

where σ is a hyper parameter, $\boldsymbol{f}_m$, $\boldsymbol{f}_n$ are feature vectors at pixels m and n, extracted from the x-ray CT image $\boldsymbol{\mu}_{CT}^{SR}$ at the super CT resolution (SR).

The PET activity image $\boldsymbol{\lambda}$ and super-resolution kernel coefficient image $\boldsymbol{\alpha}^{SR}$ are jointly estimated as:

$$\widehat{\boldsymbol{\lambda}}, \widehat{\boldsymbol{\alpha}}^{SR} = \underset{\boldsymbol{\lambda} \geq \mathbf{0}, \boldsymbol{\alpha}^{SR} \geq \mathbf{0}}{\operatorname{argmax}} \; L(\boldsymbol{y} \mid \boldsymbol{\lambda}, \boldsymbol{K}(\boldsymbol{\mu}_{CT}^{SR})\boldsymbol{\alpha}^{SR}). \tag{5}$$

The super-resolution GCT image $\boldsymbol{\mu}^{SR}$ is recovered as

$$\widehat{\boldsymbol{\mu}}^{SR} = \boldsymbol{K}(\boldsymbol{\mu}_{CT}^{SR})\widehat{\boldsymbol{\alpha}}^{SR}. \tag{6}$$

3. EVALUATION RESULTS

The existing kernel MLAA method and proposed super-resolution methods were evaluated on both physical phantom and real patient scans acquired on a uEXPLORER PET/CT system[4]. Both TOF PET data and CT scans at 80 kVp were acquired for the study.

3.1 Physical phantom results

For the phantom study, a cylindrical phantom with four inserts (for a total of five compartments) was used. The phantom was filled with water in the background and the four inserts were filled with (1) lung tissue-equivalent material, (2) water, and (3&4) salt water, as shown in Fig. 1, respectively. A ^{18}F-FDG solution was uniformly filled in all five compartments. Additional attenuation materials composed of fat tissue-equivalent material and bovine rib bones were wrapped around the phantom. The phantom was scanned with the uEXPLORER system for 30 min.

To reduce computational cost, this pilot study focused on 2D data that were synthesized from the 3D acquisition. The 2D sinogram were obtained by summing the sinograms corresponding to two adjacent detector rings. With CT-converted μ map as initial guess, GCT images were reconstructed using both the MLAA and kernel MLAA algorithms with 300 iterations at both the PET image size of 150 × 150 (4.0 mm × 4.0 mm pixel size) and the CT image size of 512 × 512 (1.17 mm × 1.17 mm pixel size). All the necessary corrections, including normalization, random and scatter corrections, have been implemented during the reconstruction.

Fig. 2 shows the reconstructed GCT images of the phantom data with both the MLAA and kernel MLAA algorithms at both the PET and CT image resolutions. Zoomed-in views of the GCT images are shown in Fig. 3. Compared to the GCT images at the PET resolution, the super-resolution GCT images had sharper edges. The kernel MLAA method showed substantially improved image quality for the super-resolution images compared to those obtained with the standard MLAA method.

3.2 Results of patient data

For patient data, a cancer patient was injected with 370 MBq of ^{18}F-FDG and scanned at 10-45 minutes post-injection on the uEXPLORER system. Fig 4. shows the 80 kVp CT image of the patient. Like the phantom study, we focused on 2D reconstructions to reduce computational cost.

Fig. 5 shows the reconstructed GCT images for the patient data with MLAA and kernel MLAA at different image resolutions. Fig. 6 shows the zoomed-in views of the GCT images with different methods at different image resolutions. We observed that the GCT images at the CT resolution revealed more structural details, for example, in the lung region, compared to the images at the PET resolution. We further computed contrast-to-noise ratio (CNR) with bone as the target region and soft tissue as the reference region. The results are shown in Fig. 7. It can be observed that kernel MLAA with the CT resolution resulted in the highest CNR compared to other methods.

4. CONCLUSION

We explored the feasibility of reconstructing super-resolution GCT images from TOF PET data at the CT image resolution. The 2D results from a physical phantom scan and a patient scan indicated that the super-resolution GCT images had sharper edges and revealed more details compared to the GCT images reconstructed at the standard PET image resolution. In

addition, the super-resolution GCT images reconstructed using the kernel MLAA method showed substantially improved image quality compared to the GCT images with the standard MLAA method.

ACKNOWLEDGEMENT

This work was supported in part by NIH R21 EB027346 and R01EB033435.

REFERENCES

[1]. Wang G, “PET-enabled dual-energy CT: image reconstruction and a proof-of-concept computer simulation study,” Phys. Med. Biol, 65(24), 245028, 2020 [PubMed: 33120376]

[2]. Li S and Wang G, “Modified kernel MLAA using autoencoder for PET-enabled dual-energy CT,” Philos. Trans. Royal Soc, 379(2204), 20200204, 2021.

[3]. Rezaei A, Defrise M, Bal G, Michel C, Conti M, Watson C, and Nuyts J, “Simultaneous reconstruction of activity and attenuation in time-of-flight PET,” IEEE Trans Med Imaging, 31(12), 2224–2233, 2012. [PubMed: 22899574]

[4]. Spencer BA et al. , “Performance evaluation of the uEXPLORER total-body PET/CT scanner based on NEMA NU 2-2018 with additional tests to characterize PET scanners with a long axial field of view,” J. Nucl. Med, 62(6): 861–870, 2021. [PubMed: 33008932]

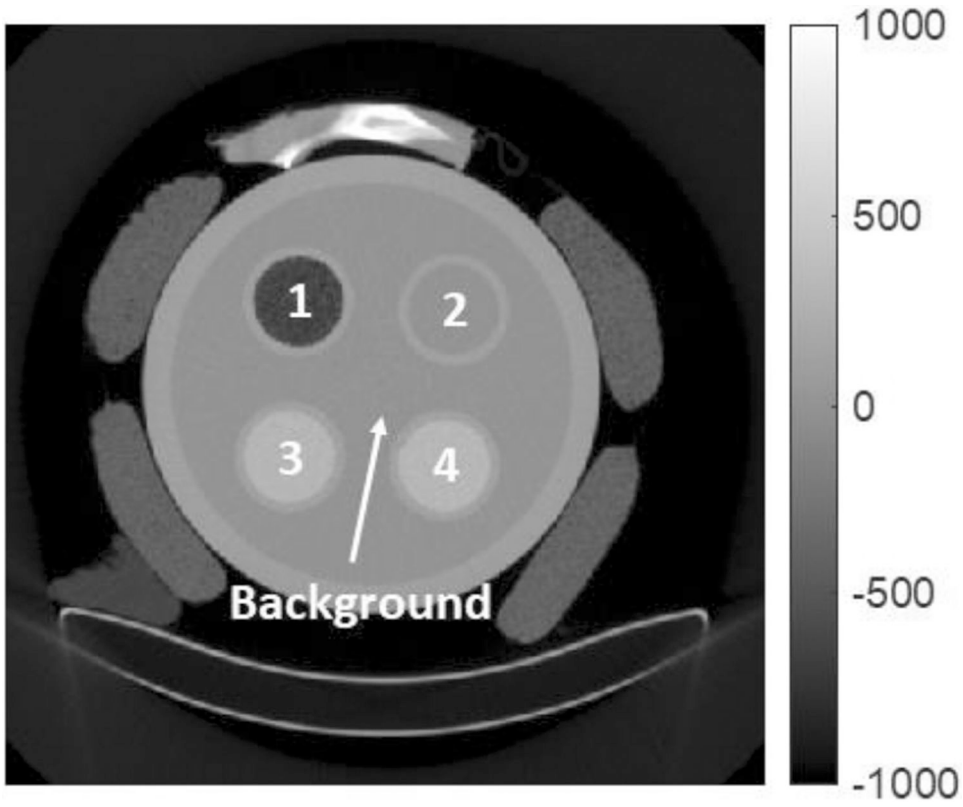

Fig. 1:
80 kVp x-ray CT images from the phantom study.

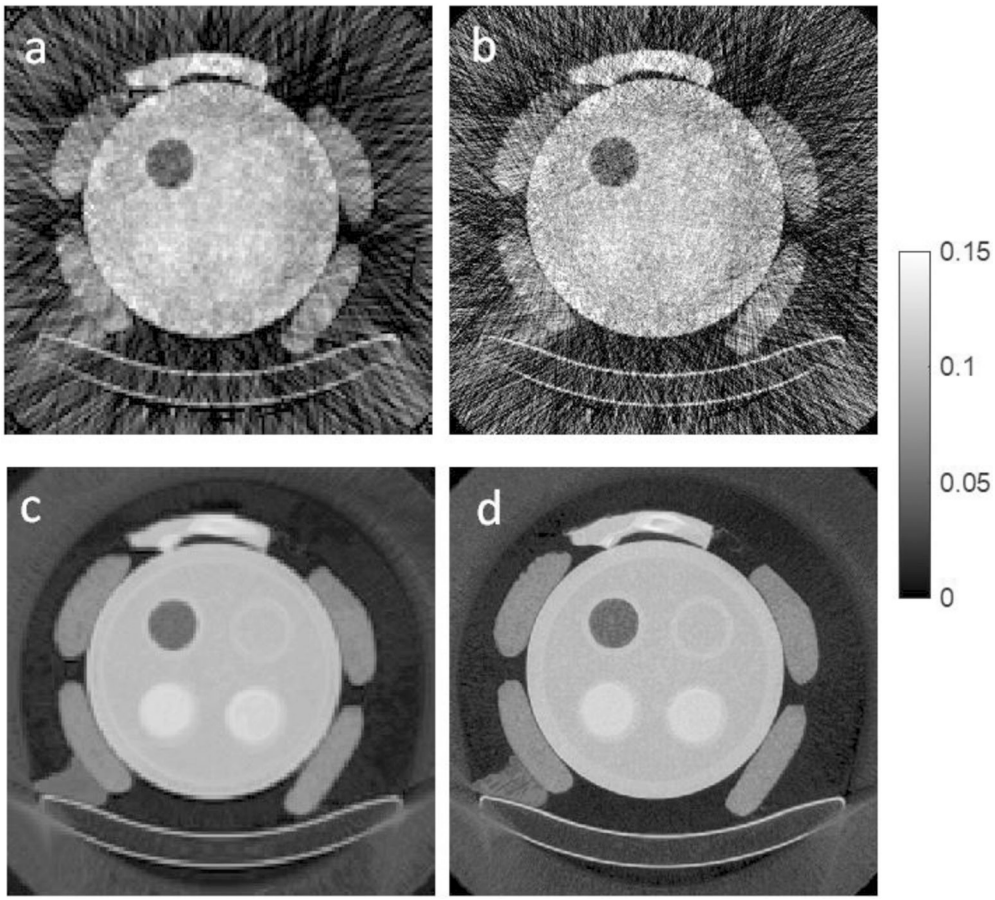

Fig. 2:

GCT images of the phantom data reconstructed with (a) MLAA at the PET resolution, (b) MLAA at the CT resolution, (c) kernel MLAA at the PET resolution, and (d) kernel MLAA at the CT resolution.

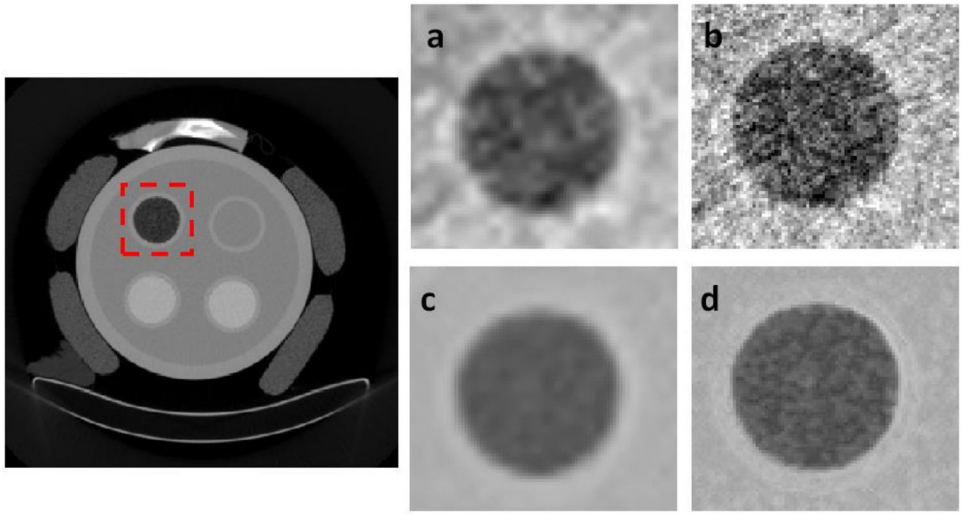

Fig. 3:

Zoomed-in view of the GCT images for the phantom data obtained with (a) MLAA at the PET resolution, (b) MLAA at the CT resolution, (c) kernel MLAA at the PET resolution, and (d) kernel MLAA at the CT resolution.

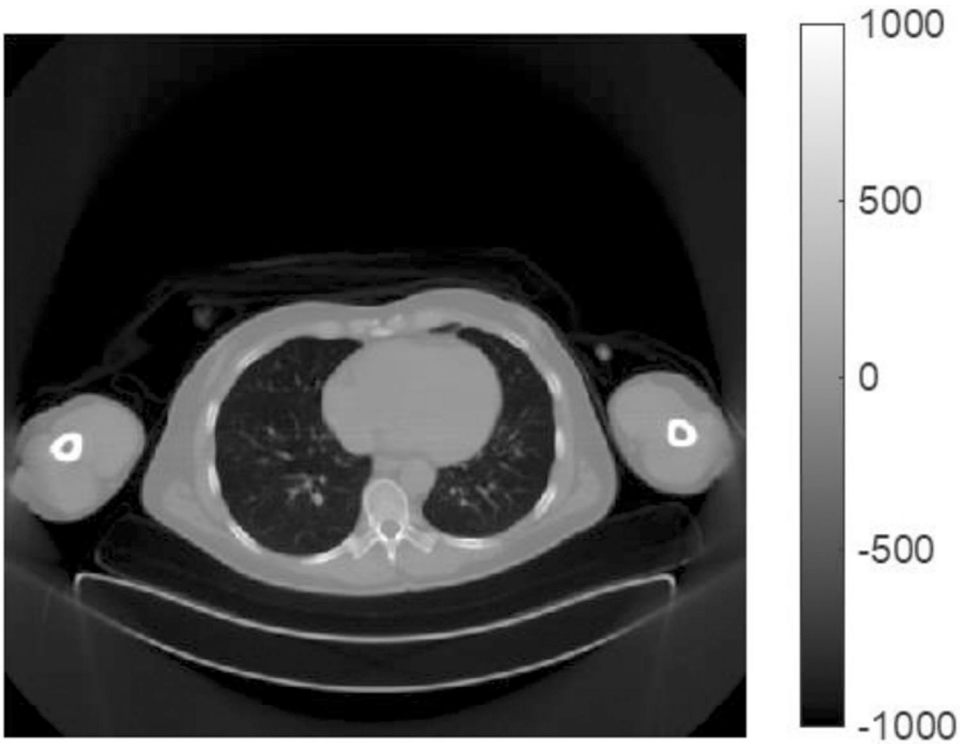

Fig. 4:
80 kVp x-ray CT images from the patient study.

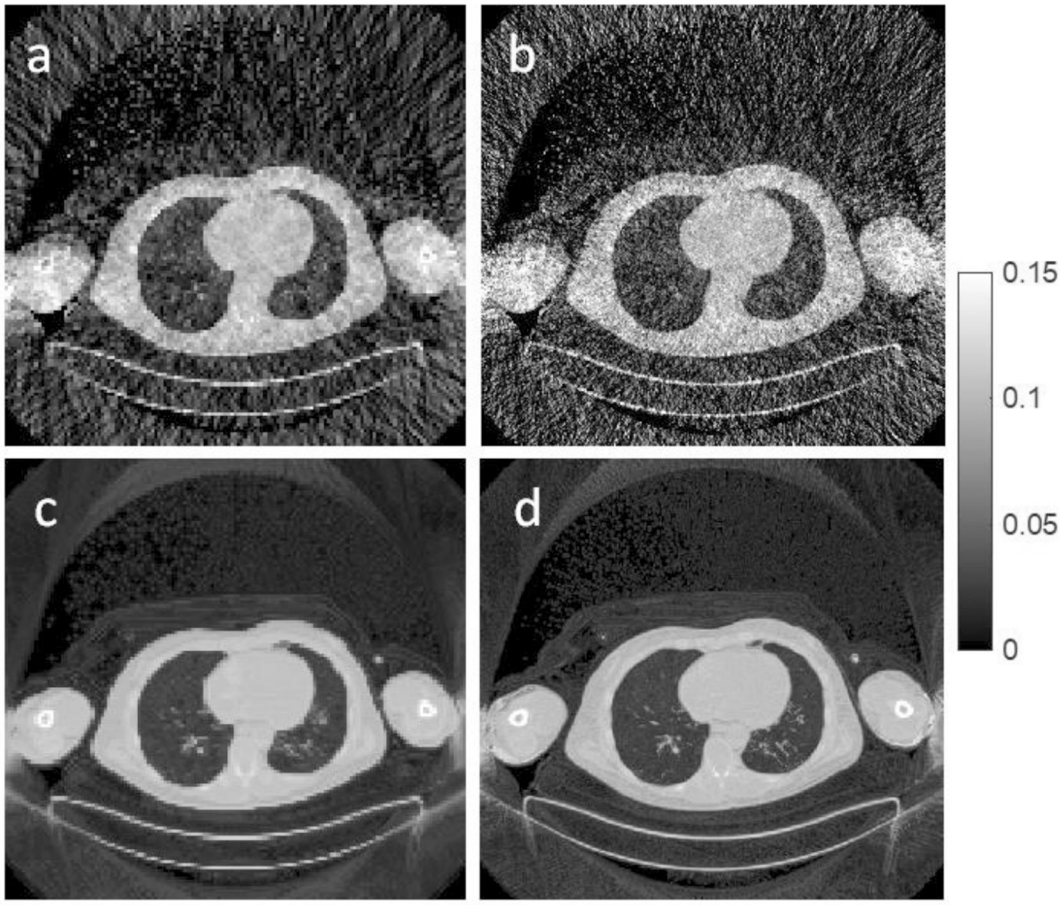

Fig. 5:
GCT images of the patient data reconstructed with (a) MLAA at the PET resolution, (b) MLAA at the CT resolution, (c) kernel MLAA at the PET resolution, and (d) kernel MLAA at the CT resolution.

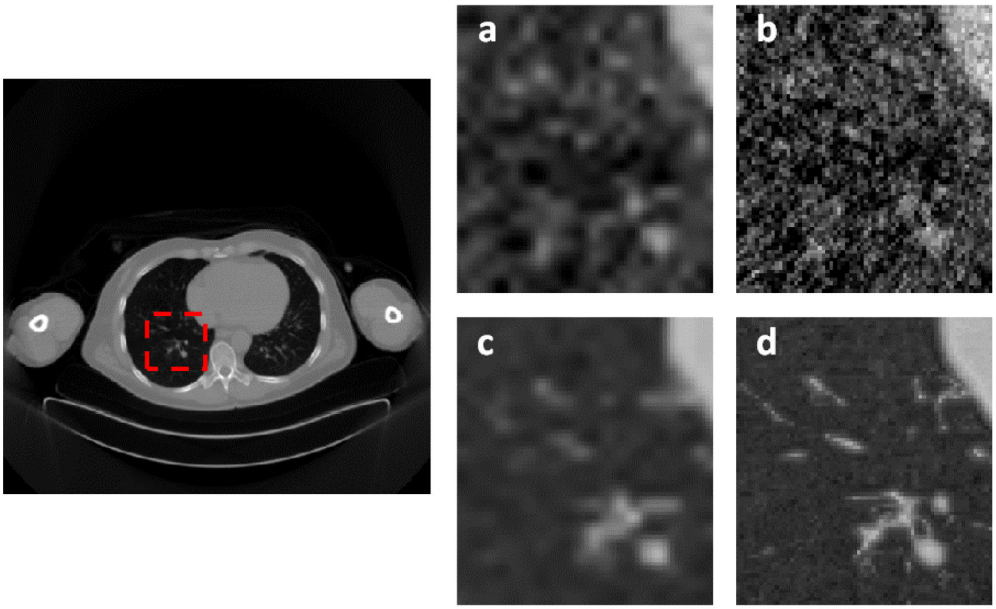

Fig. 6:
Zoomed-in view of the GCT images for the patient data obtained with (a) MLAA at the PET resolution, (b) MLAA at the CT resolution, (c) kernel MLAA at the PET resolution, and (d) kernel MLAA at the CT resolution.

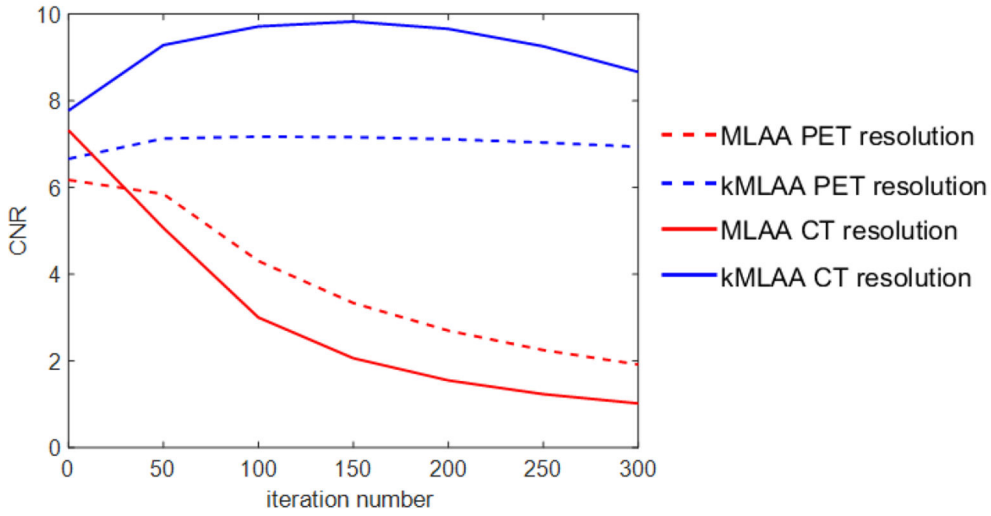

Fig. 7:

CNR vs. iteration number for the patient data obtained with the MLAA and kernel MLAA methods at different resolutions.